5

The Growth and Properties of Rare Earth-Doped $NaY(WO_4)_2$ Large Size Crystals

Chaoyang Tu*, ZhenYu You, Jianfu Li, Yan Wang and Zhaojie Zhu
Key Laboratory of Photoelectric Materials Chemistry and Physics of CAS,
Fujian Institute of Research on the Structure of Matter,
Chinese Academy of Sciences,
P.R. China

1. Introduction

Recently, strong attention has been focused on development of a new-advanced material for optoelectronics applications. $MRe(WO_4)_2$ [M=alkali metal, Re=rare earth] single crystals is noticed as an interesting self-frequency conversion solid-state laser host material because of stimulated Raman scattering[1]. $NaY(WO_4)_2$ crystal is classified among the disorder crystalline host for lasing rare-earth ions[2]. Because of the disorder structure, the optical features in the absorption and emission spectrum even at low temperature are broadened.

The lattice parameters of $NaY(WO_4)_2$ crystal are a=b=5.205 Å and c=11.251 Å respectively with the space group of $I4_1/a$ [3]. This crystal is a typical tetragonal scheelite-type crystal with a formula $MT(WO_4)_2$, where M is a monovalent alkali cation and T a trivalent cation . In these materials the M and T cations are randomly distributed in the 2b and 2d sites [4], which can be replaced by rare earth ions, such as Nd^{3+}, Yb^{3+}, Tm^{3+}, Ho^{3+} and Ce^{3+}. As a consequence, the optical absorption and emission lines of rare earth doping ions become broadened, which allow some laser tunability as well as a better match with the available diode laser emissions used for pumping. As it melts congruently, large size single crystal can be easily obtained by the Czochralski (CZ) method. Furthermore, the higher concentration of rare earth ions can be accepted in the crystal because of the higher covalent characteristic results in the lower luminescent quenching efficiency. Compared to the other laser host crystals such as YAG and YVO_4 crystal, $NaY(WO_4)_2$ crystal has lower melting point and its raw materials for crystal growth is in-nocuity. As a result, $NaY(WO_4)_2$ crystal can serve as an excellent laser host. In this chapter, the crystal growth, thermal characteristic, optical and spectrum and laser properties of rare earth doped- $NaY(WO_4)_2$ crystals are presented.

2. The growth of large size crystals

Rare earth-doped $NaY(WO_4)_2$ crystals were grown in air along <001> direction by using Czochralski method[1~3]. The chemicals used were analytical grade Na_2CO_3, WO_3, Y_2O_3 and spectral grade Re_2O_3 (Re=Yb, Tm, Ho,Ce, Nd, Er). The starting materials were prepared by mixing Y_2O_3, Na_2CO_3, WO_3 and Re_2O_3 powders according to reaction formula:

$$Na_2CO_3+(1-x)Y_2O_3+x\ Re_2O_3+4WO_3 \rightarrow 2NaY_{1-x}Re_x(WO_4)_2+CO_2\uparrow$$

The weighed materials with doping 6 at% Re^{3+} were thoroughly mixed and pressed and put into a platinum crucible with Φ50×50 mm^3, then heated to 750 °C and kept for 18 h to decompose the Na_2CO_3, and ground, mixed again, and then reheated to 800 °C, kept for 24 h. The obtained sample was very hard ceramics.

The synthesized material melted congruently at 1210 °C. The platinum crucible was heat by conventional RF-heating method. Crucible size is 50 mm in diameter and 50 mm in height. The pulling rate was 1-1.5 mm/h and the crystal rotation rate at 12-20 r.p.m. To release the stress produced in the temperature-lowering process, the crystals were annealed at 1200 °C for 5-6 h and then cooled down to room temperature at a rate of 20 K/h.

The earlier grown crystals as shown in Fig.2.1 occur screwy crack during anneal process. In order to avoid the cracking of the crystal, the designed after-heater should be used and the above crystal must be taken to anneal again in O_2 atmosphere according to a special temperature-controlled procedure.

As a result, high-quality (Tm^{3+},Ho^{3+},Nd^{3+},Yb^{3+},Er^{3+}/Yb^{3+}) rare earth doped-NYW cylinder crystal with dimension of Φ25 mm×100 mm (shown in Fig.2.2~2.5). The result shows that its optical homogeneity is 4×10^{-5}, as shown in Fig.2.5. It shows that it has excellent quality.

In order to obtain the large-sized rare earth doped-$NY(WO_4)_2$ crystals with high optical homogeneity, the control of growing processes and conditions are very important firstly. Then the used raw materials must be highly pure. Furthermore, to get the defined composition of the melt, the preparation of chemicals was found to be important. Thirdly, the seed surface must be melted to remove the defect in the seed before growing. And the growth point temperature must be a little higher than the saturation point. The control of the pulling rate, rotating rate and annealing rate is also very important. Finally, a designed after-heater should be used to avoid the crack of large crystal.

The concentration of rare earth ions in the $NaY(WO_4)_2$ crystal has been measured to by the inductively coupled plasma-atomic emission spectrometry (ICP-AES) method. A sample for the experiment has been cut from the top to eh boule. The concentration of Yb^{3+} ions has been 1.73 wt%. The distribution coefficient (K_0) of Yb^{3+} ions in the Yb:$NaY(WO_4)_2$ crystal has been calculated using the following relation:

$$K_0=C_A / C_0 ;$$

Where C_A is the Yb concentration at the top of the grown crystal and C_0 is the initial concentration of the admixture. The result indicates that the segregation coefficient of Yb^{3+} ions in Yb: $NaY(WO_4)_2$ crystal is approximately 1.02.

3. The thermal characteristic

The a and c axes were obtained by the YX-2 X-ray Crystal Oridentation Unit (produced by Dandong Radiative Instrument Co,Ltd). Two pieces of square samples with the size 5×5×5 mm^3 having polished faces perpendicular to the a and c crystallophysical directions were used to carry out the measurements. The thermal expansion of as-grown Yb^{3+}:$NaY(WO_4)_2$ crystal was measured by using Diatometer 402 PC instrument from 300 K to 1273 K[1]. Because of the relatively lower reliability of the room temperature cell parameter arising out of presence of water in the sample chamber, only the data from 473 to 1273 K is considered

in calculating the expansion coefficients. The thermal expansion pattern was obtained (shown in the Fig.3.1). The thermal expansion coefficients of the Yb^{3+}:$NaY(WO_4)_2$ crystal were calculated over different temperature ranges. In this case, the linear thermal expansion coefficients for different crystallographic direction c- and a-axes are , 1.83×10^{-5} K^{-1}, 0.85×10^{-5} K^{-1}, respectively.

Fig. 2.1 The cracking Nd^{3+}:$NaY(WO_4)_2$ crystal.

Fig. 2.2 The grown Nd^{3+}:$NaY(WO_4)_2$ crystal.

Fig. 2.3 The grown Yb^{3+}:$NaY(WO_4)_2$ crystal.

Fig. 2.4 The grown Re^{3+}:$NaY(WO_4)_2$ crystals (Re=Yb, Nd,Er/Yb).

Fig. 2.5 The grown Re^{3+}:$NaY(WO_4)_2$ crystals (Re=Tm/Ho).

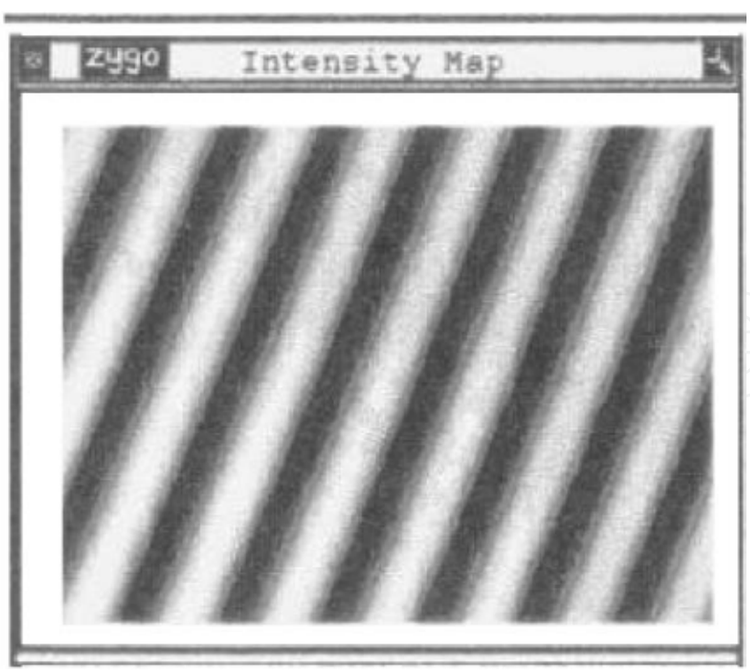

Fig. 2.6 Interference fringe of crystals.

The thermal-expansion coefficient $\left[\alpha_{ij}\right]$ of a crystal is a symmetrical second-rank tensor and it can be described by the representation quadric. The $NaY(WO_4)_2$ crystal belongs to the tetragonal system and 4/m point group. The unique symmetry axis is a fourfold axis along the crystallographic c-axis; the axes of the crystallographic and crystallophysical coordinate systems in $NaY(WO_4)_2$ have the same direction. In this case the value of thermal expansion along a- and b-axis are comparable and the values of α_1 and α_3 can be obtained by measuring the thermal expansion of the a- and c-oriented crystal.

The expansion coefficient in the [001] is about two times larger than that of the [100] direction according to our experimental results, which means that the $NaY(WO_4)_2$ crystal has anisotropic thermal expansion. The reason for the themal expansion coefficient along the c-axis being larger than that along the a- or b-axis can be explained by the structure of the $NaY(WO_4)_2$ crystal. The $NaY(WO_4)_2$ crystal has a scheelite structure according to the XRPD experiment results. According to Fig.3.1, it can be seen that there are five layers and three layers perpendicular to the c- and the a- or b-axis, respectively. According to the XRPD experiment results, the distance of the interlayer of five layers and three layers are c/4 and a/2 (or b/2),which is equal to 2.813×10^{-10} and 2.603×10^{-10} m, respectively. The larger the distance of the interlayer is, the weaker the chemical bonds of the interlayer will be according to the crystal lattice vibration dynamics. It can be seen that the interaction force along the c-axis is weaker than that along the a- or b-axis, and there are more layers in the c-direction than in the a-direction. Thus when the crystal is heated, the thermal expansion of the Yb^{3+}:$NaY(WO_4)_2$ crystal along the c-axis is larger than that along the a- or b-axis.

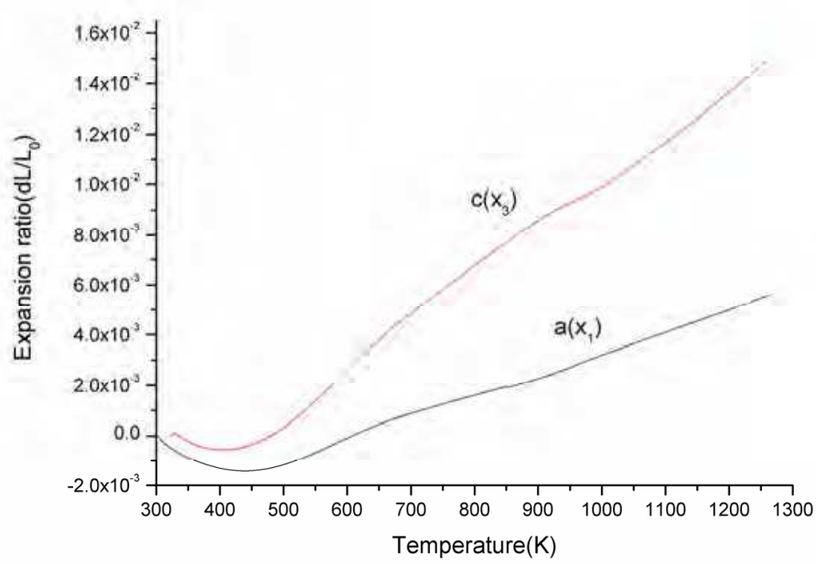

Fig. 3.1 The curve of thermal expansivity of $Yb:NaY(WO_4)_2$.

4. The spectroscopic characteristics

4.1 The spectroscopic characteristic of Nd^{3+}: $NaY(WO_4)_2$ crystal

Fig.4.1 shows the RT absorption spectrum of Nd^{3+}:$NaY(WO_4)_2$ Crystal. Owing to the disordered structure and the high Nd-doping concentration, the strong absorption intensity and broad FWHM of every band are shown, especially for the 806 nm[1]. Its FWHM is about 16 nm and the cross-section is about 2.8×10^{-20} cm^2 at 806 nm, which is benefit to the pumping of commercial laser diode. Fig.4.2 shows the RT emission spectrum with the pumping perpendicular to (001) planes. There are six emission peaks at follows wavelength: 894, 917,1063,1087,1339 and 1389 nm. The value of emission cross-section at 1063 nm is about 4.6×10^{-20} cm^2. Fig.4.3 shows the fluorescence decay of $^4F_{3/2}$ level of Nd^{3+} in NYW crystal at RT and the lifetime of $^4F_{3/2}$ level is about 85 μs and relative luminescent quantum efficiency is about 47% . Tab.4.1 presents the integrated absorbance, the line strengths, the experimental and calculated oscillator strengths. Table 4.2 shows the calculated radiative probabilities, radiative branching ratios and radiative time for the emissions from the $^4F_{3/2}$ level of Nd^{3+}:NYW crystal. Table 4.3-4 give the comparison of spectrum parameters in Nd:NYW and other Nd-doped crystals.

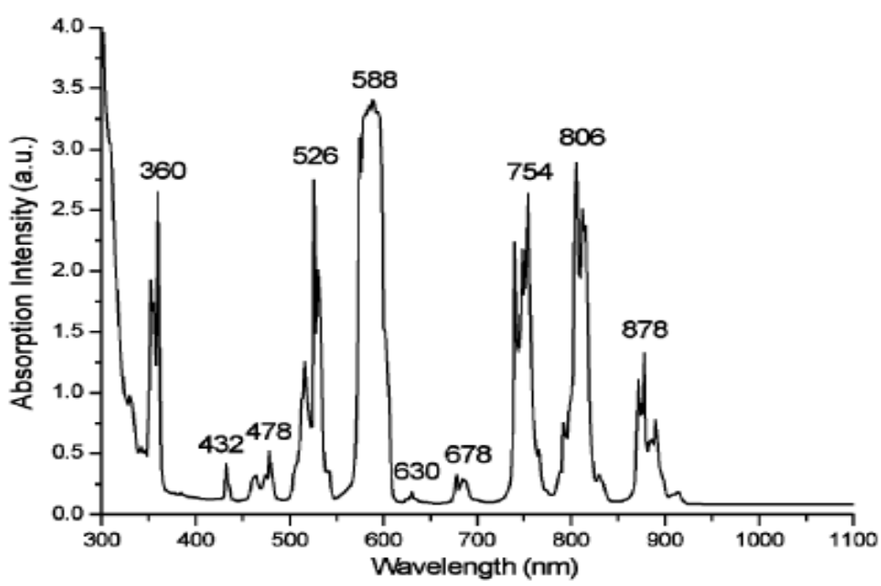

Fig. 4.1 Absorption spectra of Nd:$NaY(WO_4)_2$ crystal.

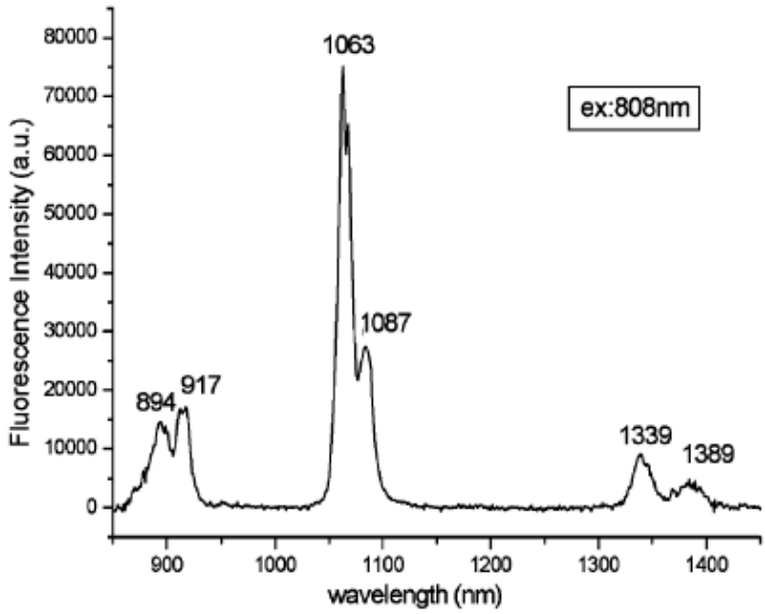

Fig. 4.2 Fluorescence spectra of Nd:NaY$(WO_4)_2$ crystal.

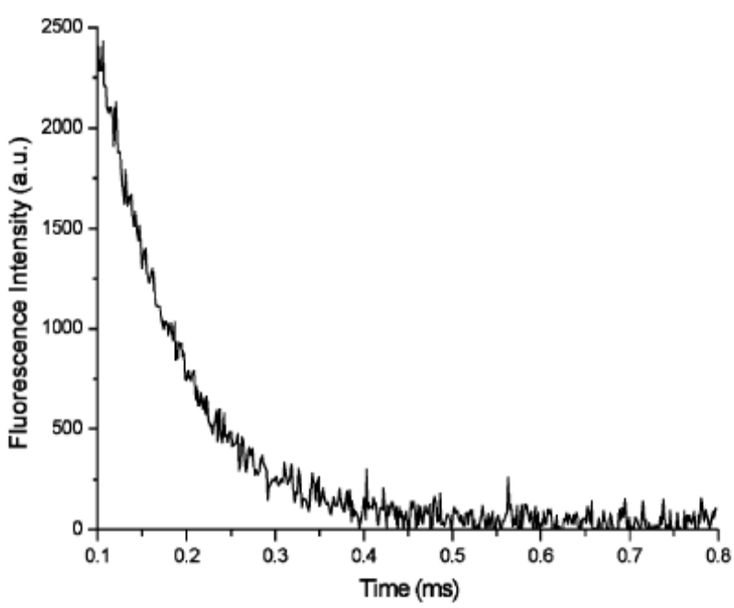

Fig. 4.3 Fluorescence decay of Nd:NYW crystal at RT.

Excited state	Wavelength (nm)	Γ (nm/cm)	S_{mea} ($10^{-29}cm^2$)	S_{cal} ($10^{-29}cm^2$)	f_{exp} (10^{-6})	f_{cal} (10^{-6})
$^4D_{1/2}+^4D_{3/2}+^5D_{5/2}$	360	71.2	2.862	3.127	15.874	17.342
$^2P_{1/2}$	432	4.57	0.153	0.221	0.708	1.021
$^2K_{13/2},,^2G_{9/2},,^2P_{3/2},,^2G_{11/2}$	478	18.42	0.558	0.416	2.329	1.739
$^4G_{7/2}+^4G_{9/2}+^2K_{13/2},$	526	130.86	3.600	2.186	13.666	8.296
$^4G_{5/2}+^2G_{7/2}$	588	375.88	9.251	9.345	31.412	31.732
$^2H_{11/2}$	630	1.47	0.034	0.061	0.107	0.193
$^4F_{9/2}$	678	10.2	0.218	0.238	0.641	0.702
$^4F_{7/2}+^4S_{3/2}$	754	159.94	3.070	3.115	8.129	8.249
$^4F_{5/2}+^2H_{9/2}$	806	191.84	3.444	3.681	8.532	9.118
$^4F_{3/2}$	878	78.2	1.289	1.554	2.931	3.533

Table 4.1 The integrated absorbance, the line strengths, the experimental and calculated oscillator strengths of Nd:NYW crystal.

Start levels	Wavelength(nm)	A(S^{-1})	β	τ (μs)
$^4I_{9/2}$	894	2612	0.473	180
$^4I_{11/2}$	1063	2434	0.441	
$^4I_{13/2}$	1339	450	0.082	
$^4I_{15/2}$	1852	23	0.004	

Table 4.2 Calculated radiative probabilities, radiative branching ratios and radiative time for the emissions from the $^4F_{3/2}$ level of Nd^{3+}:NYW crystal.

Crystal	Ω_2 (10^{-20} cm^2)	Ω_4 (10^{-20} cm^2)	Ω_6 (10^{-20} cm^2)	FWHM (nm)	σ_a at 808 nm (10^{-29} cm^2)	*Ref.*
Nd:NYW	5.8	5.74	4.32	16	2.80	[1]
Nd:NBW	30.9	12	9.3	10	2.6	[2]
Nd:KYW	8.80	3.11	3.16	8	3.13	[3]
Nd:KGW	12.67	10.15	7.48	12	26	[4,5]
Nd:YVO_4	5.88	4.08	5.11	8	27	[6]
Nd:$GdVO_4$	12.629	4.828	8.425	4.7	9.396	[7]
Nd:YAG	0.2	2.7	5.0	0.9	7.0	[8,9]
Nd:YAP	0.69	3.69	4.56	3	10.2	[10,11]
Nd:GAB	3.118	2.676	5.343	8.7	4.3	[12]

Table 4.3 Comparison of spectral values in Nd:NYW and other Nd-doped crystals.

Crystal	σ_e at 1064nm (10^{-20} cm^2)	τ_f (μs)	η (%)	References
Nd:NYW	4.56	85	47	[1]
Nd:NBW	16	122	85	[2]
Nd:KYW	4.5	154	78.6	[3]
Nd:KGW	38	110	92.4	[4,5]
Nd:YVO_4	100	98	46.8	[6]
Nd:$GdVO_4$	7.6	90	45.5	[7]
Nd:YAG	34	240	91	[8,9]
Nd:YAP	24.4	180.4	88	[10,11]
Nd:GAB	30	55.6	19	[12]

Table 4.4 Comparison of the emission spectroscopic parameters of some Nd-doped laser crystal.

4.2 The spectroscopic characteristic of Yb^{3+}: $NaY(WO_4)_2$ crystal

Fig.4.4 shows the RT Polarized absorption spectrum of Yb^{3+}:$NaY(WO_4)_2$ Crystal. The largest absorption cross-section is located at 976 nm in the $\sigma-$ and $\pi-$ spectrum, which is the main pump wavelength of the possible Yb^{3+} laser in $NaY(WO_4)_2$ crystal using the InGaAs LD, and the value is 1.81×10^{-20} cm^{-2}. This value is smaller than that of Yb^{3+}:$KY(WO_4)_2$ (13.3×10^{-20}) crystals at 981 nm [13], but larger than those of Yb^{3+}:YAG crystal (0.8×10^{-20} cm^2) [14] at 942 nm and Yb^{3+}:YCOB crystal (1.0×10^{-20} cm^2) [15] at 976nm. Fig.4.5 shows the RT Polarized emission spectrum of Yb^{3+}:$NaY(WO_4)_2$ Crystal. The emission cross-sections of crystal calculated from the fluorescence spectra by the reciprocity method and the Füchtbauer-Ladengurg formula are shown in Fig.4.6 [16~18]. The radiative lifetime τ_r of the $^2F_{3/2}$ manifold is measured to be 0.902 ms. The gain coefficient was calculated for several values of population inversion $\boldsymbol{P}$ ($\boldsymbol{P}$=0, 0.1, 0.2…) and is shown in Fig.4.7 (a) and Fig.4.7 (b). Positive gain coefficient for $\boldsymbol{P}$ values larger than 0.5, which are encountered in a free-running laser operation, implies a tuning range from 990 to 1070 nm.

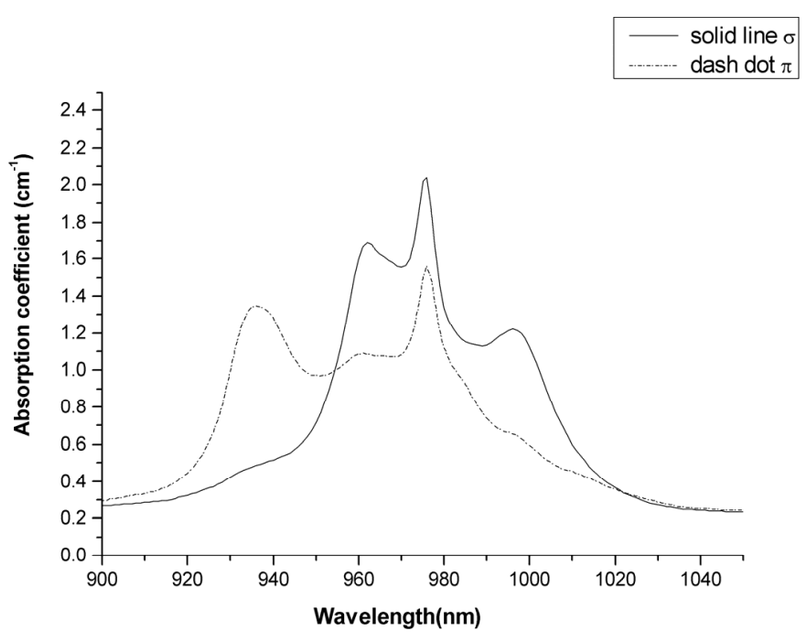

Fig. 4.4 Polarized absorption spectra of Yb:$NaY(WO_4)_2$ crystal.

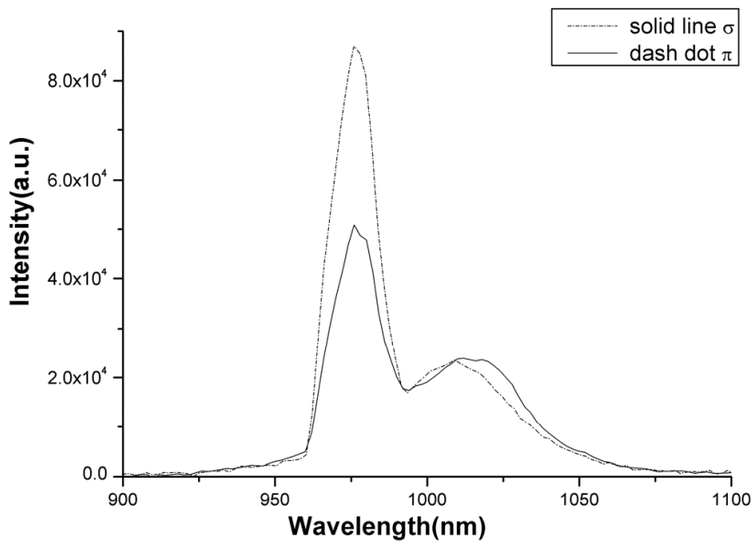

Fig. 4.5 Polarized fluorescence spectra of $Yb:NaY(WO_4)_2$ crystal.

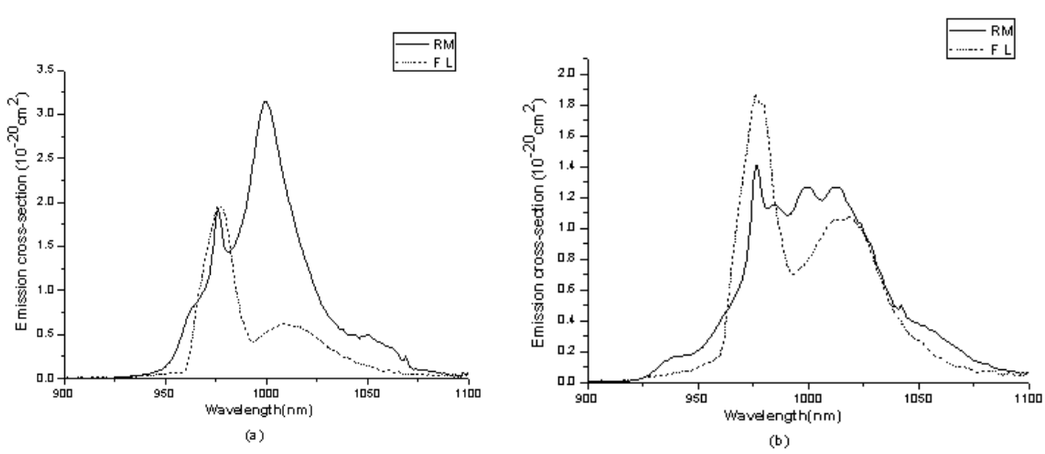

Fig. 4.6 The emission cross-sections of crystal calculated from the fluorescence spectra by the reciprocity method and the Füchtbauer-Ladengurg formula.

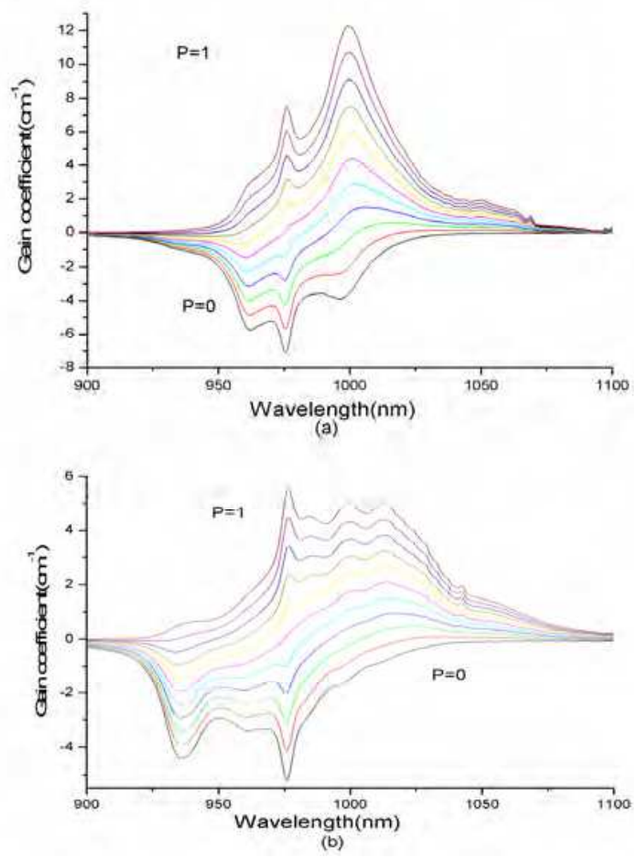

Fig. 4.7 The gain coefficient was calculated for several values of population inversion $\boldsymbol{P}$ ($\boldsymbol{P}$ =0, 0.1, 0.2…).

4.3 The spectroscopic properties of Tm^{3+}, Ho^{3+}: $NaY(WO_4)_2$ crystal

Fig.4.8 shows the Room temperature absorption spectra of Tm^{3+}-, Ho^{3+}-doped and Tm^{3+}/Ho^{3+} co-doped $NaY(WO_4)_2$ crystals (a) in the range 300-850 nm and (b) in the range 1100-2100 nm. The spectrum of Tm^{3+}: $NaY(WO_4)_2$ crystal consists of six resolved bands associated with the transitions from the $^3H_6$ ground state to the $^3F_4$, $^3H_5$, $^3H_4$, $^3F_{2,3}$, $^1G_4$ and $^1D_2$ excited states. It can be seen that the absorption band of the σ polarization is narrower and has a larger peak cross section than the π absorption band. The spectrum of Ho^{3+}: $NaY(WO_4)_2$ crystal consists of ten resolved bands associated with the transitions from the $^5I_8$ ground state to the $^5I_7$, $^5I_6$, $^5F_5$, $^5F_4$+$^5S_2$, $^5F_3$, $^3K_8$+$^5F_2$, $^5F_1$+$^5G_6$, $^5G_5$($^3G_5$),, $^3H_6$+$^5F_2$+$^3H_5$ and $^3K_6$+$^3F_4$+$^3H_4$+$^3G_4$ excited states[19]. Some absorption bands of Tm^{3+} and Ho^{3+} ions overlap in the Tm^{3+}/Ho^{3+}:$NaY(WO_4)_2$ crystal. Compared to Ho^{3+} ions concentration in Ho^{3+}: $NaY(WO_4)_2$ and Tm^{3+} ions concentration in Tm^{3+}/Ho^{3+}:$NaY(WO_4)_2$ crystal, the concentration of Ho^{3+} ions in Tm^{3+}/Ho^{3+}:$NaY(WO_4)_2$ crystal is very low; the $^5I_8 \rightarrow {}^5I_7$ (Ho^{3+}) transition of Tm^{3+}/Ho^{3+}:$NaY(WO_4)_2$ crystal is extremely weak.

Fig.4.9 shows the absorption cross sections and polarized stimulated emission cross sections associated with the (a) $^3F_4 \rightarrow {}^3H_6$ transition for the Tm^{3+}:$NaY(WO_4)_2$ and (b) $^5I_7 \rightarrow {}^5I_8$ for Ho^{3+}:$NaY(WO_4)_2$ crystal derived by the reciprocity method. The maximum values of σ_{em}

are 1.399×10^{-20} cm² for σ polarization at 2044 nm and 1.426×10^{-20} cm² for π polarization at 2047 nm. For comparison, the σ_{em} obtained for Tm^{3+} in NLuW are $2.0(\pm0.1)\times10^{-20}$ cm² at 1798 nm and $1.9(\pm0.1)\times10^{-20}$ cm² at 1830nm, respectively[20] . The FWHMs of the emission bands for σ and π polarizations are 161 and 130 nm, respectively.

Fig.4.10 presents the gain cross-section calculated for different values of P (P=0.1~0.5) for (a) the $^3F_4\rightarrow{}^3H_6$ transition of Tm^{3+} in $NaY(WO_4)_2$ crystal and (b) the $^5I_7\rightarrow{}^5I_8$ transition of Ho^{3+} in $NaY(WO_4)_2$ crystal. The gain curves at a wavelength longer than 1900 nm are obscure due to the low signal-to-noise ratio of the absorption spectrum. The positive gain cross-section can be obtained at about 2.0 μm when P exceeds 0.2. The positive gains for P=0.5 are in a range from 1758 to about 1954 nm for σ polarization and from 1758 to about 1977 nm for π polarization, respectively.

Fig.4.11 presents the room temperature fluorescence spectra of Tm^{3+}-, Ho^{3+}-doped and Tm^{3+}/Ho^{3+} co-doped $NaY(WO_4)_2$ crystals.

Fig.4.12 gives the decay curves of $^3F_4$ manifold in the samples of bulk and powder in the Tm^{3+} doped $NaY(WO_4)_2$ crystals. Fig.4.13 also gives the decay curves of Ho: $^5I_7$ level in the (a) samples of bulk and powder in the Ho^{3+}:$NaY(WO_4)_2$ and (b) Tm, Ho:$NaY(WO_4)_2$ crystals.

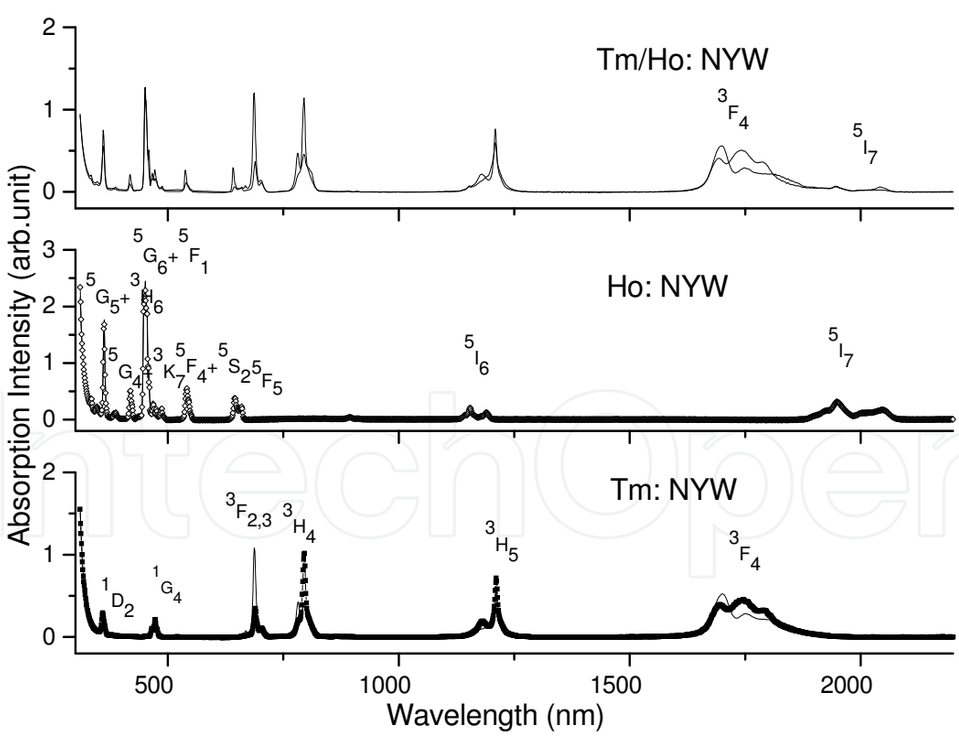

Fig. 4.8 Room temperature absorption spectra of Tm^{3+}-, Ho^{3+}-doped and Tm^{3+}/Ho^{3+} co-doped $NaY(WO_4)_2$ crystals.

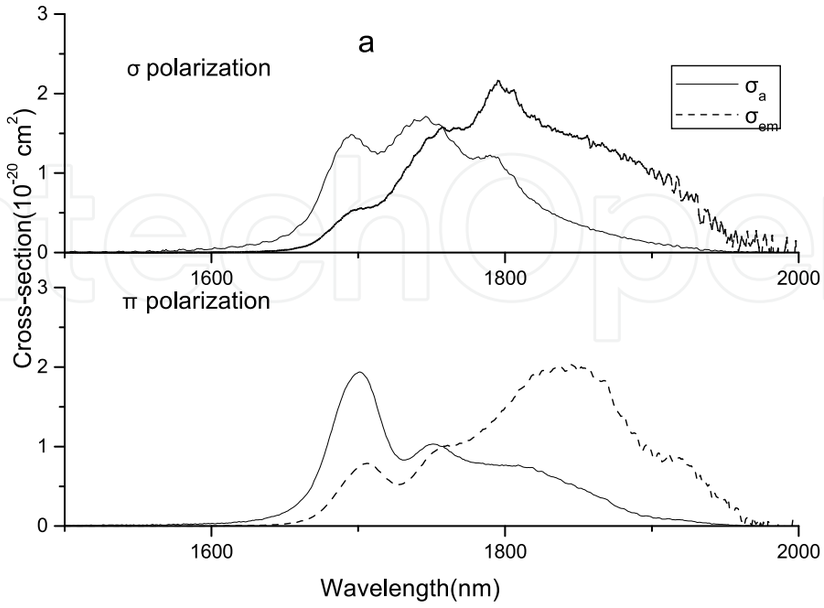

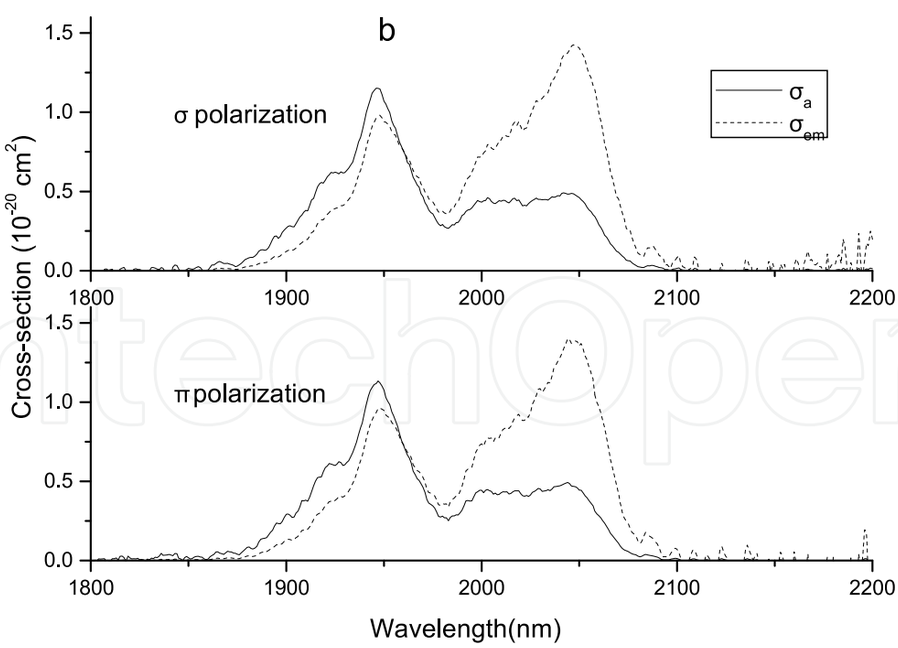

Fig. 4.9 Absorption cross sections and polarized stimulated emission cross sections associated with the (a) $^3F_4 \rightarrow {}^3H_6$ transition for the Tm^{3+}:$NaY(WO_4)_2$ and (b) $^5I_7 \rightarrow {}^5I_8$ for Ho^{3+}:$NaY(WO_4)_2$ crystal derived by the reciprocity method.

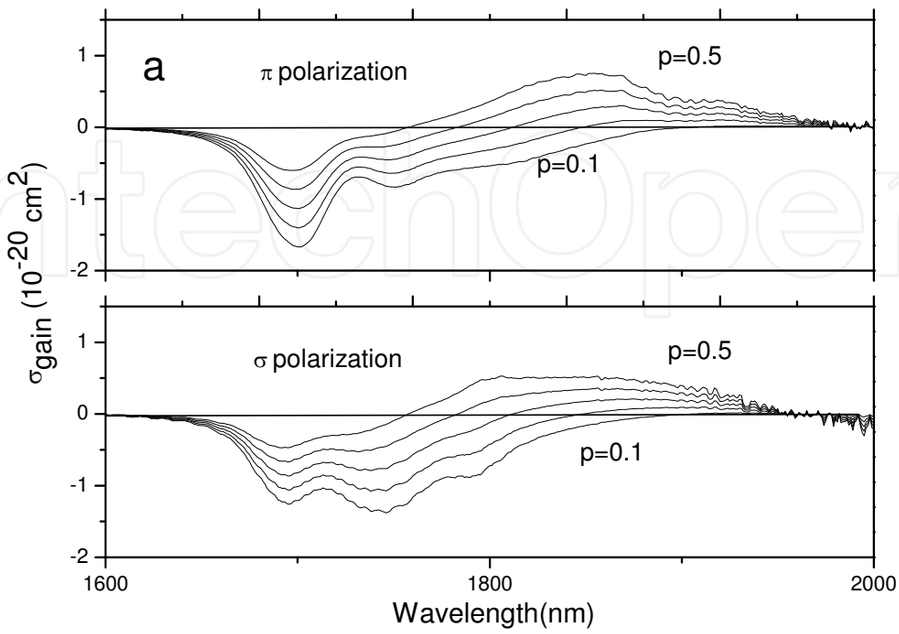

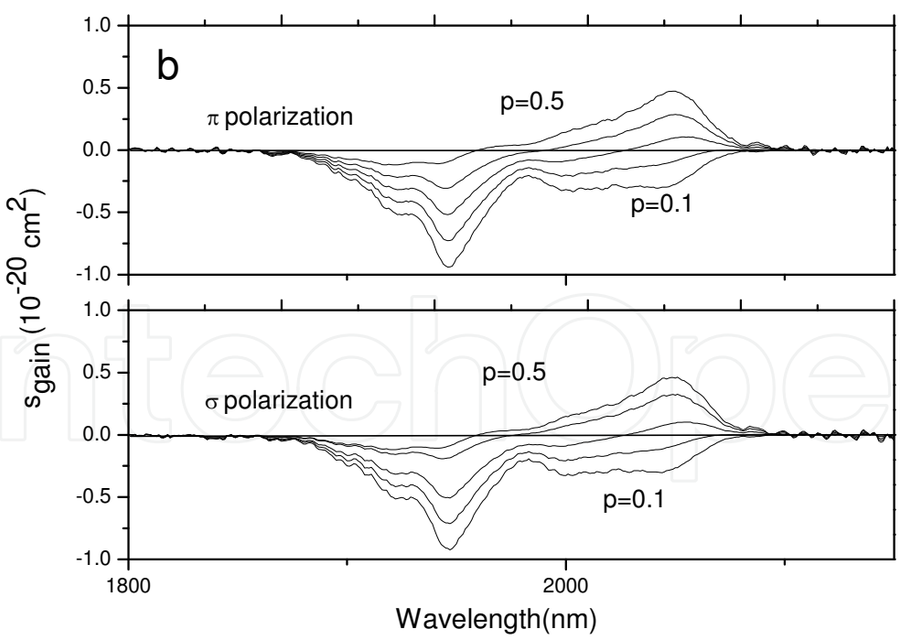

Fig. 4.10 Gain cross-section calculated for different values of P (P=0.1~0.5) for (a) the $^3F_4 \rightarrow {}^3H_6$ transition of Tm^{3+} in $NaY(WO_4)_2$ crystal ,(b) the $^5I_7 \rightarrow {}^5I_8$ transition of Ho^{3+} in $NaY(WO_4)_2$ crystal.

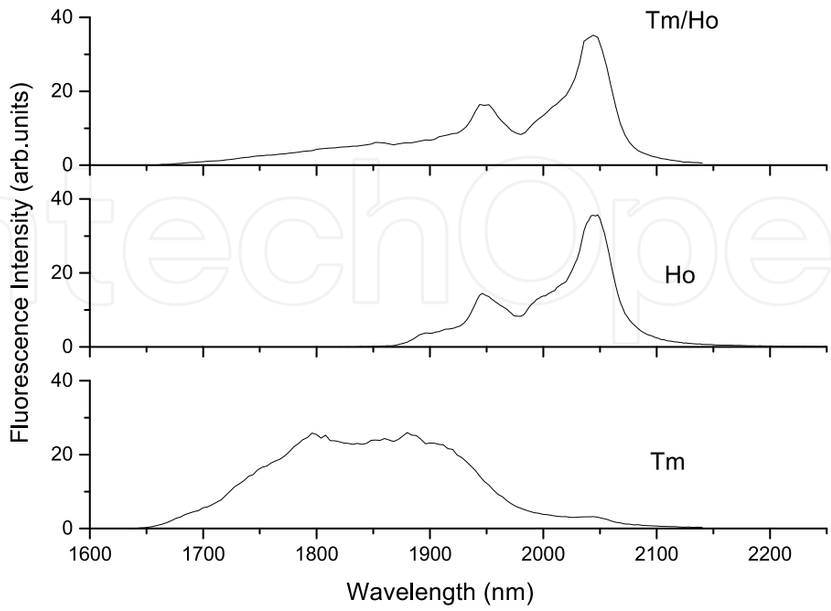

Fig. 4.11 Room temperature fluorescence spectra of Tm^{3+}-, Ho^{3+}-doped and Tm^{3+}/Ho^{3+} co-doped $NaY(WO_4)_2$ crystals.

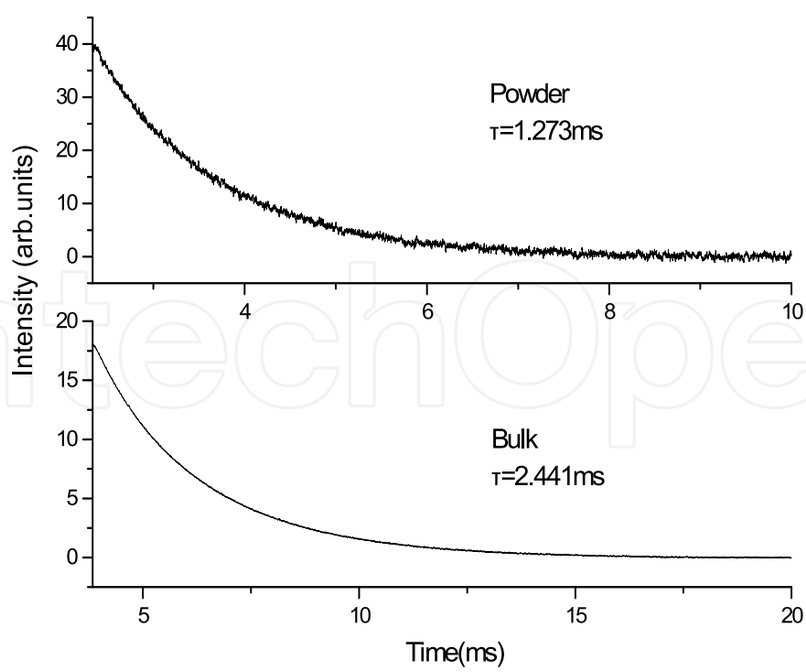

Fig. 4.12 Decay curves of $^3F_4$ manifold in the samples of bulk and powder in the Tm^{3+} doped $NaY(WO_4)_2$ crystals.

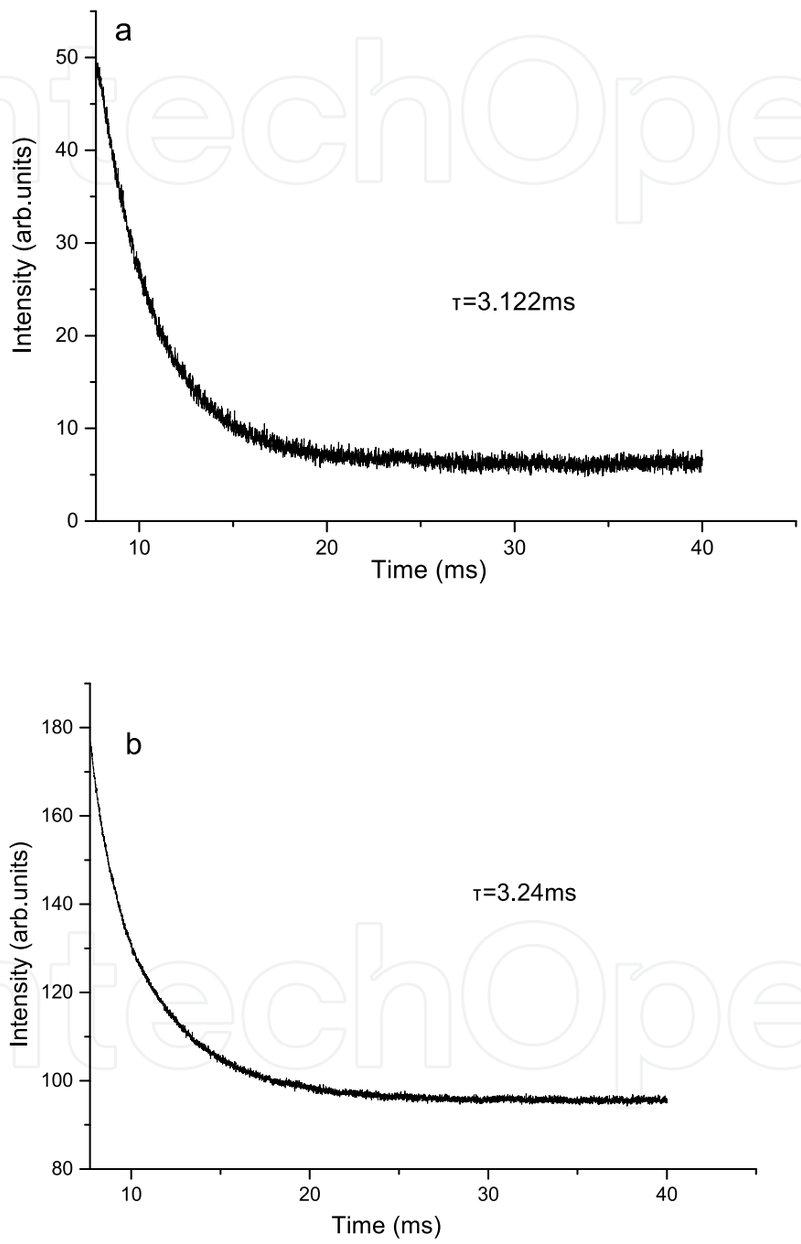

Fig. 4.13 Decay curves of Ho: $^5I_7$ level in the (a) samples of bulk and powder in the Ho^{3+}: $NaY(WO_4)_2$ and (b) Tm, Ho: $NaY(WO_4)_2$ crystals.

5. The laser characteristics

5.1 The laser characteristics of Nd^{3+}: $NaY(WO_4)_2$ crystal

The Nd^{3+}:$NaY(WO_4)_2$ crystal was made into laser stick and the laser experiment was performed using a xenon flash lamp as a pump source[1]. Maximum pulse energy of 786 mJ with a repetition rate of 1 Hz has been obtained. A maximum output power of 87 mW at 532 nm has been obtained and the double-frequency conversion efficiency is more than 25% when a LBO optical crystal was used as the frequency-doubling crystal. Table 5.1 shows the data of input and output energy and Fig.5.1 presents the relationship between the Iuput energy and output energy. Table 5.2 presents the Comparison of laser properties of Nd:NYW crystal and Nd:YAG crystal. It can be found that the Nd:NYW crystal has the higher laser efficiency than Nd:YAG crystal. Table.5.3 shows the frequency-doubling laser output power and conversion efficiency and Fig.5.2 presents the relationship between the pump power and output power of SH generation. Fig.5.3 shows the laser facula of the SH generation.

Input V（J）	static state output（mJ）	Wavelength（μm）
440 （9.68）	7	1.063
480 （11.5）	33	
520 （13.5）	67	
560 （15.7）	106	
600 （18.0）	173	
640 （20.5）	215	
680 （23.1）	275	
720 （25.9）	346	
760 （28.9）	376	
800 （32.0）	443	
840 （35.3）	512	
880 （38.7）	572	
920 （42.3）	671	
960 （46.1）	735	
1000（50）	786	

Table 5.1 Data table of pumping energy and output energy.

Crystal	Size	Input	Output
Nd:NYW Crystal	Φ4.5 mm×52 mm	50 J	786 mJ
Nd:YAG Crystal	Φ8 mm×120 mm	50 J	~800 mJ

Table 5.2 Comparison of laser properties of Nd:NYW and Nd:YAG.

Input	Output/530nm	Threshold	Optical to optical efficiency for SHG	Slope efficiency	Optical to optical efficiency for ground frequency
1500 mW	87 mW	410 mW	5.80%	7.98%	> 25%

Table 5.3 SH generation power and conversion efficiency.

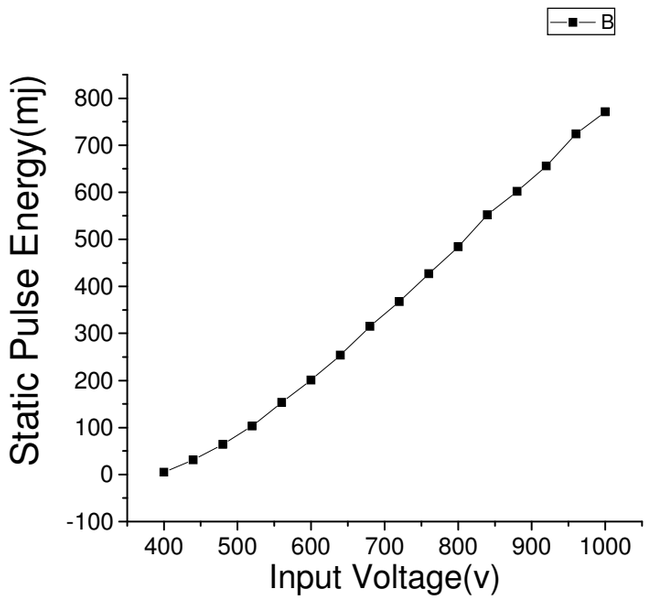

Fig. 5.1 The relationship between the Iuput energy and output energy at 1.062 um.

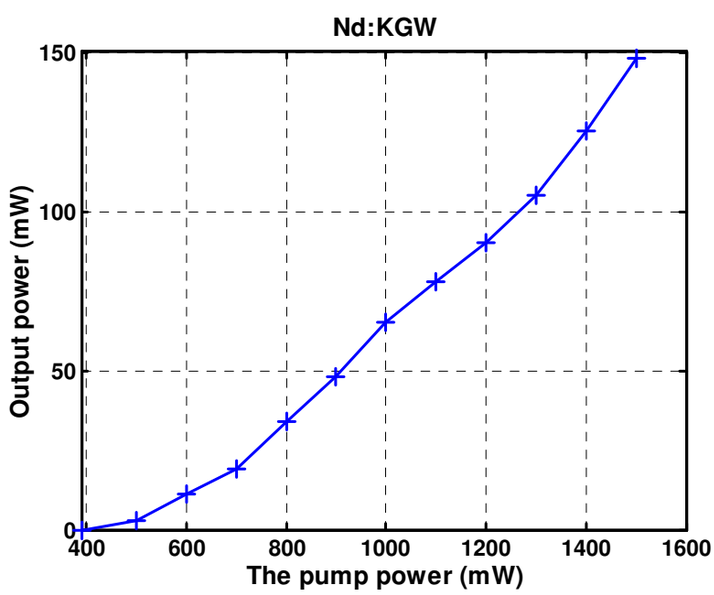

Fig. 5.2 The relationship between the pump power and output power of SH generation.

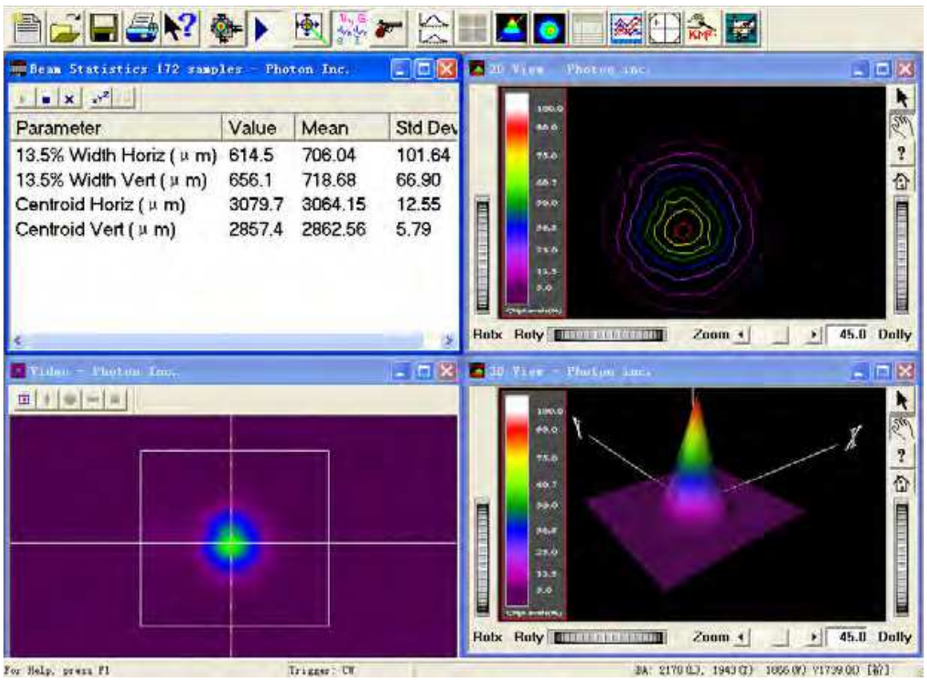

Fig. 5.3 The laser facula of the SH generation.

5.2 The laser characteristics of Tm, Ho: $NaY(WO_4)_2$ crystal

An infrared laser output at 2.07 μm with Tm, Ho:$NaY(WO_4)_2$ crystal end-pumped by 795 nm laser diode at room temperature is reached[2,3]. Fig.5.4 shows the experimental configuration of the LD-end-pumping Tm, Ho: NYW laser. The crystal used with the concentrations of 5 at% Tm^{3+} and 1 at% $Ho^{3+}$was grown by the Czochralski method. The highest output power was up to 2.7 W corresponding to the crystal temperature being controlled at 283 K. Fig.5.5 presents the output power versus pumping power at different temperatures. The overall optical conversion efficiency was 5.4% and the slop efficiency was 26%. The output characteristics and the laser threshold affected by the pulse duration and temperature have been studied. It can be found that the stability of the output power was correlative with the crystal temperature heavily. In addition, the wider pulse duration of pump could promote the output power efficiently as shown in Fig.5.6, which presents the output power versus pulse duration.

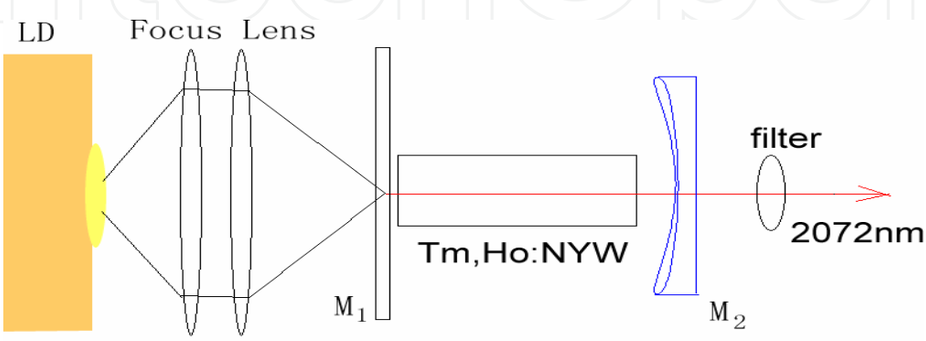

Fig. 5.4 The experimental configuration of the LD-end-pumping Tm, Ho: NYW laser.

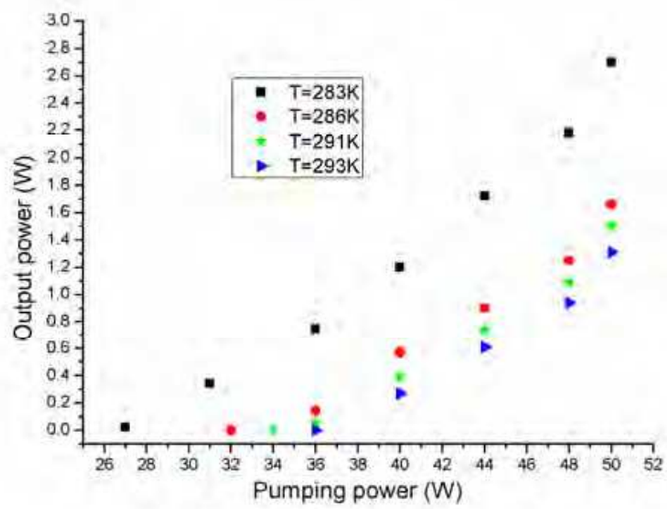

Fig. 5.5 The output power versus pumping power at different temperatures.

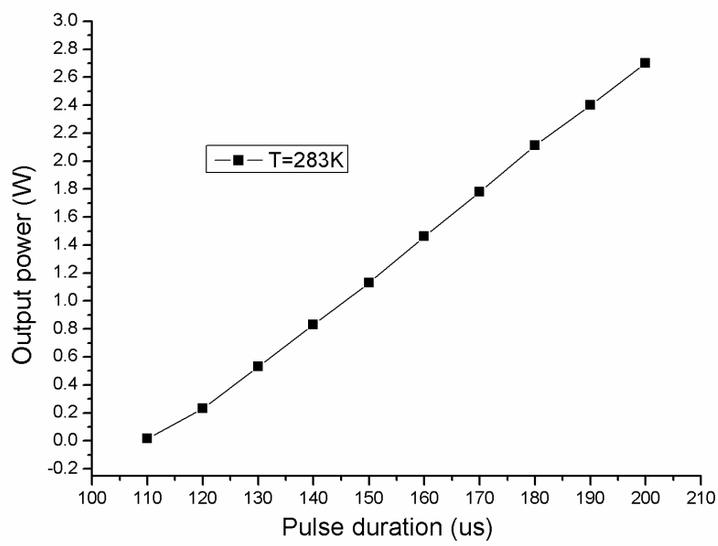

Fig. 5.6 The output power versus pulse duration.

With Ti:sapphire laser pumping at 795 nm, a slope efficiency and a maximum output power as high as 48% and 265 mW, respectively, have been obtained at 2050 nm from a Tm:Ho: $NaY(WO_4)_2$ crystal by Prof.C.Zaldo[4]. Tuning from 1830 nm to 2080 nm has also been achieved using an intracavity Lyot filter. Fig.5.7 shows Cw laser performance of Tm(5 at%), Ho(0.25 at%): $NaY(WO_4)_2$ crystal. Fig.5.8 shows Cw and quasi Cw laser performance of Tm(5 at%), Ho(0.5 at%): $NaY(WO_4)_2$ crystal.

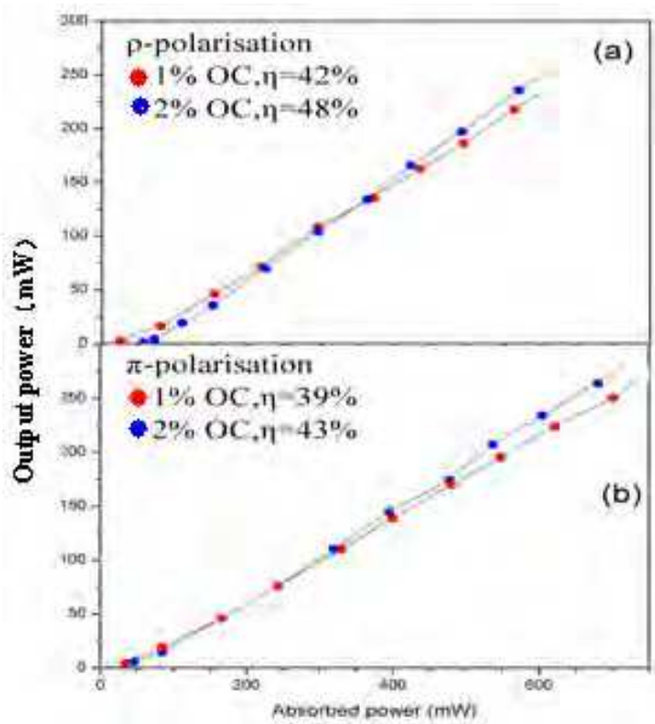

Fig. 5.7 Cw laser performance of Tm(5 at%),Ho(0.25 at%): $NaY(WO_4)_2$ crystal. (a) σ -pol (1.55-mm-long crystal).(b) π -pol (3.4-mm-long crystal).

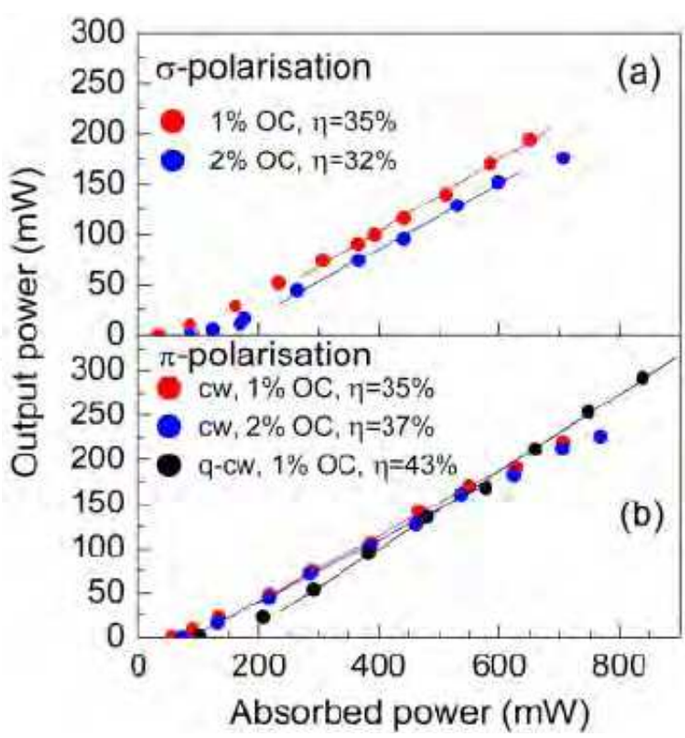

Fig. 5.8 Cw and quasi Cw laser performance of Tm(5 at%),Ho(0.5 at%): $NaY(WO_4)_2$ crystal. (a) σ -pol (1.75-mm-long crystal).(b) π -pol (3.5-mm-long crystal).

Prfo.A.A.Lagatsky and C.Zaldo [5] also reported the femtosecond-pulse operation of a $Tm:Ho:NaY(WO_4)_2$ laser at around 2060 nm by using an ion-implated InGaAsSb quantum-well-based semiconductor saturable absorber mirror for passive mode-locking maintenance for the first time. Transform-limited 191fs pulses are produced with an average output power of 82 mW at a 144 MHz pulse repetition frequency. Maximum output power of up to 155 mW is generated with a corresponding pulse duration of 258 fs. Fig.5.9 presents the Input-output characteristics of the mode-locked $Tm:Ho:NaY(WO_4)_2$ laser.

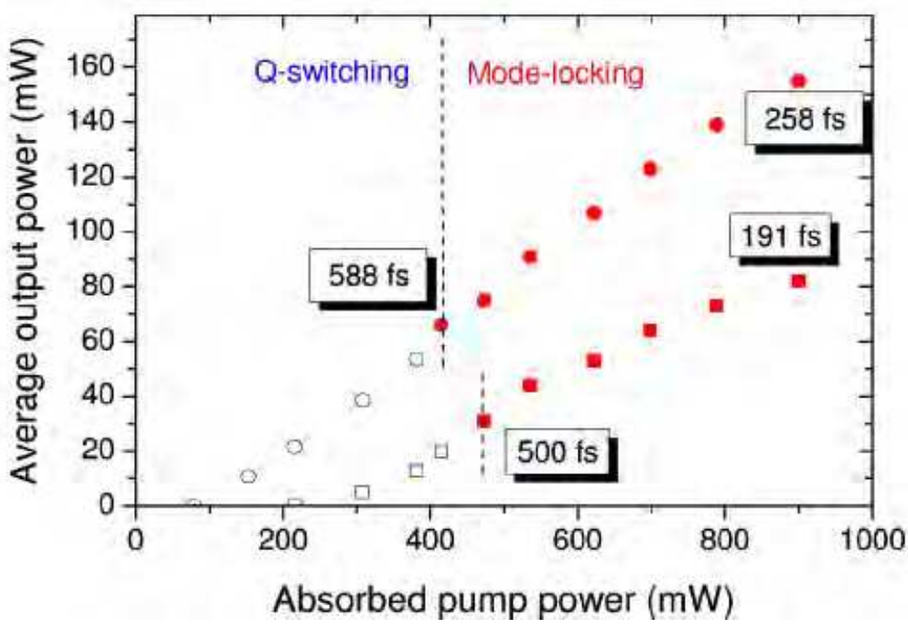

Fig. 5.9 Presents the Input-output characteristics of the mode-locked $Tm:Ho:NaY(WO_4)_2$ laser.

Two different operation regimes, shorter-pulse and higher-power, are indicated by squares and circles, respectively. Q-switching and mode-locking regimes are represented by open and closed symbols, respectively.

5.3 The laser characteristics of Tm, Ho, Ce: $NaY(WO_4)_2$ crystal

An infrared laser output at 2.07 μm with $Tm,Ho,Ce:NaY(WO_4)_2$ single crystal end-pumped by 795 nm laser diode at room temperature[3,6]. The crystal used with the concentrations of 5 at% Tm^{3+}, 1 at% Ho^{3+} and 30 at% Ce^{3+} was grown by the Czochralski method. The highest output power was up to 0.2 W corresponding to the pumping power of 50 W and the threshold was about 40 W at 293 K. Figure 5.10 shows the output power versus the pump power. The introduction of Ce^{3+} brought about a novel phenomenon. End-pumping with the 795 nm LD, it was found the up-conversion was repressed heavily and the green emission disappeared thoroughly in $Tm,Ho,Ce:NaY(WO_4)_2$ crystal, which was particularly different from the crystal $Tm,Ho:NaY(WO_4)_2$, where the green emission was obvious and weakened the sensitized transition energy.

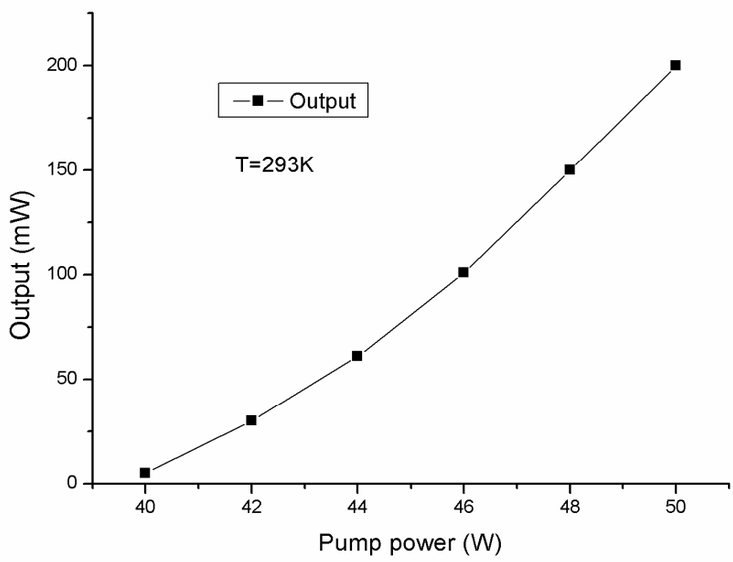

Fig. 5.10 The output power versus the pump power.

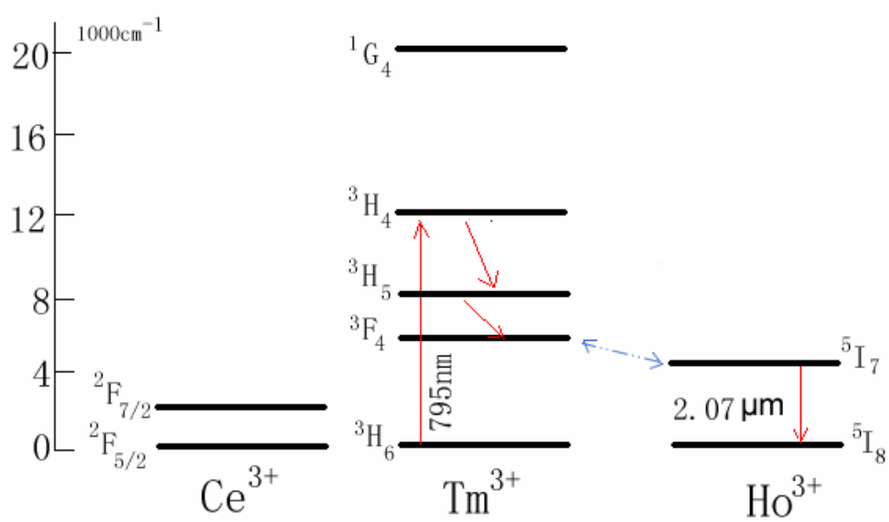

Fig. 5.11 The illustration of Ce^{3+}, Tm^{3+}, Ho^{3+} energy levels.

The original intention of selecting the Ce^{3+} was to compensate the up-conversion loss. The compensation mechanisms of the Ce^{3+} lie in its transition energy. As shown in Fig.5.11, the transition energy of $^2F_{7/2}\rightarrow{}^2F_{5/2}$ (Ce^{3+}) is close to that of $^3H_5\rightarrow{}^3F_4$ (Tm^{3+}) and half of the

$^3H_4 \rightarrow {}^3H_5$ (Tm^{3+}). Pumped with 795 nm, the electrons will transit from $^3H_6$ to $^3H_4$, and jump to $^3H_5$, $^3F_4$ depending on the radiationless transition. Because the energy level $^3F_4$ (Tm^{3+}) was close to $^5I_7$ (Ho^{3+}), the electrons will transit from $^3F_4$ (Tm^{3+}) to $^5I_7$ (Ho^{3+}), which is just the sensitized process. At last, the transition $^5I_7 \rightarrow {}^5I_8$ (Ho^{3+}) generates the2.07 μm laser. In the complex sensitized process, only few of the electrons will transit from the upper pumping energy level $^3H_4$ (Tm^{3+}) into the $^5I_7$ (Ho^{3+}), which is the reason of the lower laser efficiency. By virtue of the Ce^{3+}, the electrons of the $^3H_4$ (Tm^{3+}) can transit fast into the energy level $^3F_4$ (Tm^{3+}). More important, the multiple transition energy can guide the electrons towards $^3F_4$ (Tm^{3+}) instead of irregular radiationless transition. That is to say, in the shorter time, there are more electrons gathering into the energy level $^5I_7$ (Ho^{3+}), which is just the demand of the high laser efficiency. Here, in our experiment, the disappeared green emission is the certification of the function of the Ce^{3+}, which contributes to the improvement of the 2 μm laser.

6. Conclusion

In this review, the growth of rare earth (Tm^{3+},Ho^{3+},Nd^{3+},Yb^{3+}, Er^{3+}/Yb^{3+})-doped $NaY(WO_4)_2$ large crystal with the dimensions of Φ25 mm×100 mm is reported. The thermal, optical and spectrum characteristics of these crystals are presented. The laser characteristics of Nd^{3+};Tm^{3+}/Ho^{3+}:$NaY(WO_4)_2$ laser crystals are also covered. Maximum pulse energy of 786 mJ with a repetition rate of 1Hz has been obtained from Nd^{3+}-doped $NaY(WO_4)_2$ crystal pumped by xenon flash lamp. It can be found that the Nd:NYW crystal has the higher laser efficiency than Nd:YAG crystal. An infrared laser output of 2.7 W at 2.07 μm with Tm,Ho:$NaY(WO_4)_2$ crystal end-pumped by 795 nm laser diode at room temperature is also reached. Furthermore, the femtosecond-pulse operation of a Tm:Ho:$NaY(WO_4)_2$ laser at around 2060 nm is obtained for the first time. Transform-limited 191fs pulses are produced with an average output power of 82 mW at a 144MHz pulse repetition frequency. Maximum output power of up to 155 mW is generated with a corresponding pulse duration of 258 fs. Also, it is found that the co-doped Ce^{3+} can depress the green up-conversion emission of Tm^{3+} and thus improves the 2 μm laser. All the above performances demonstrate that $NaY(WO_4)_2$ crystal can serve as an excellent laser host.

7. Acknowledgements

Some works of this chapter were supported by National Nature Science Foundation of China (No.50902129, 61078076), Major Projects from FJIRSM (SZD09001), the Knowledge Innovation Program of the Chinese Academy of Sciences (Grant No. KJCX2-EW-H03), Science and Technology Plan Major Project of Fujian Province of China (Grant No. 2010I0015).

8. References

1.
[1] Z.X. Cheng, S.J. Zhang, J.R. Han, et al.,, Cryst. Res. Technol. 36 (2001) 135;
[2] A.A. Kaminskii, H.J. Eichler, K. Ueda,, et al., Appl. Opt. 38 (1999) 4533;
[3] Z. L. Zhu, Y. N. Qian, J. H. Liu,et al., J. Cera. Soci. 35(2007) 991-994;
[4] C. Cascales, M. D. Serrano, F. Esteban-Betegón, et al.,, Phys. Rev. B. 74(2006) 174114;

2.
[1] Yan Wang,Chaoyang Tu, Zhenyu You, et al.,Journal of Crystal Growth, 285(1-2)2006:123-129;
[2] Chengli Sun, Fugui Yang, Ting Cao, et al., Journal of Alloys and Compounds, 509(25)(2011): 6987-6993;
[3] Zhenyu You, Master dissertation, The study of Nd^{3+} and Yb^{3+} doped in $NaY(WO_4)_2$ and Cr^{3+}doped in $LiNbO_3$ crystals,Graduated School of Chinese Academy of Sciences,2010.
3.
[1] Zhenyu You, Master dissertation, The study of Nd^{3+} and Yb^{3+} doped in $NaY(WO_4)_2$ and Cr^{3+}doped in $LiNbO_3$ crystals,Graduated School of Chinese Academy of Sciences,2010.
4.
[1] Yan Wang,Chaoyang Tu, Zhenyu You, et al.,Journal of Crystal Growth, 285(1-2)2006:123-129;
[2] A. Mendez-Blas, M. Rico, V. Volkov, et al., Mol. Phys. 101 (2003): 941.
[3] X. Han and G. Wang, J. Crystal Growth 247 (2003):551.
[4] Y. Kalisky, L. Kravchik and C. Labbe, Opt. Commun. 189 (2001): 113.
[5] R. Moncorge, B. Chambon, J.Y. Rivorie,et al., Opt. Mater. 8 (1997):109.
[6] M.H. Randles, J.E. Creamer and R.F. Belt, OSA technical digest ser. Opt. Soc. Am. 10 (1998): 289.
[7] H.D. Jiang, H.J. Zhang, J.Y. Wang, et al., Opt. Commun. 198 (2001):447.
[8] W.F. Krupke, IEEE J. Quantum Electron. QE-7 (1991):153.
[9] W. Koechner, Solid state laser engineering, Optical Science (third ed.), Springer Verlag, New York (1992).
[10] H. Zhang, Z. Luo, A. Zhen, C.M. Wu and G.S. Li, Chin. J. Infrared Res. A 7 (1998): 297.
[11] A.A. Kaminskii, Laser crystals. In: H.F. Ivey, Editor, Springer, Berlin, Heidelberg, New York (1981).
[12] C.Y. Tu, Master dissertation, Study on the blue–green laser crystal Nd3+:GdxY1−xAl3 $(BO_3)_4$, Graduated School of Chinese Academy of Sciences, 2001.
[13] N.V. Kuleshov, A.A. Lagatsky, A.V. Podlipensky, et al., Opt.lett.22(1997)1317.
[14] K.I. Schaffers, L.D. Deloach, S.A. Payne, IEEE J. Quantum electron. 32 (1996) 741.
[15] H.Zhang, X.Meng, P. Wang, et al., Appl. Phys. B 68 (1999) 1147.
[16] K. Ohta, H. Saito, M. Obara, J. Appl. Phys. 73,(1993) 3149.
[17] D.E. McCumber, Phys. Rev. A 134(1964) 299.
[18] S.A. Payne, L.L. Chase, L.K. Smith, et al., IEEE J. Quantum Electron. QE-28 (1992) 2619.
[19] W.T. Carnall, P.R. Fields, K. Rajnak, J Chem Phys, 49 (1968) 4424.
[20] X. M. Han, J. M. Cano-Torres, M. Rico,et al., J. Appl. Phys. 103(2008) 083110.
5.
[1] Zhenyu You, Master dissertation, The study of Nd^{3+} and Yb^{3+} doped in $NaY(WO_4)_2$ and Cr^{3+}doped in $LiNbO_3$ crystals,Graduated School of Chinese Academy of Sciences,2010.
[2] F. G. Yang, C. L. Sun, Z. Y. You, et al., Laser Phys.20(2010)1695;
[3] Fugui Yang, Doctoral dissertation, The study of LD pumped yellow and 2μm laser properties, Graduated School of Chinese Academy of Sciences,2011.
[4] X.Han, F.Fusari, M.D.Serrano, et al. OPTICS EXPRESS 18(6)(2010)5413;
[5] A.A.Lagatsky, X.Han, M.D.Serrano, et al. OPTICS LETTERS 35(18)(2010)3027;
[6] F.G. Yang, F.P. Yan, Z.Y. You, et al., Laser Phys. Lett. 7(2010)867.

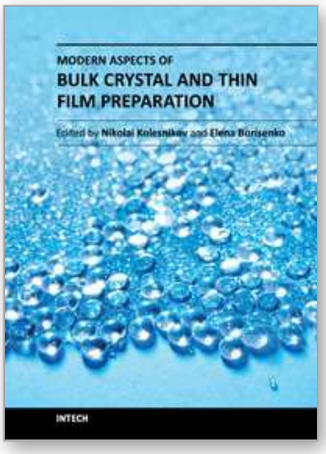

Modern Aspects of Bulk Crystal and Thin Film Preparation

Edited by Dr. Nikolai Kolesnikov

ISBN 978-953-307-610-2

Hard cover, 608 pages

Publisher InTech

Published online 13, January, 2012

Published in print edition January, 2012

In modern research and development, materials manufacturing crystal growth is known as a way to solve a wide range of technological tasks in the fabrication of materials with preset properties. This book allows a reader to gain insight into selected aspects of the field, including growth of bulk inorganic crystals, preparation of thin films, low-dimensional structures, crystallization of proteins, and other organic compounds.

How to reference

In order to correctly reference this scholarly work, feel free to copy and paste the following:

Chaoyang Tu, ZhenYu You, Jianfu Li, Yan Wang and Zhaojie Zhu (2012). The Growth and Properties of Rare Earth-Doped NaY(WO4)2 Large Size Crystals, Modern Aspects of Bulk Crystal and Thin Film Preparation, Dr. Nikolai Kolesnikov (Ed.), ISBN: 978-953-307-610-2, InTech, Available from: http://www.intechopen.com/books/modern-aspects-of-bulk-crystal-and-thin-film-preparation/the-growth-and-properties-of-rare-earth-doped-nay-wo4-2-large-size-crystals

INTECH
open science | open minds

InTech Europe
University Campus STeP Ri
Slavka Krautzeka 83/A
51000 Rijeka, Croatia
Phone: +385 (51) 770 447
Fax: +385 (51) 686 166
www.intechopen.com

InTech China
Unit 405, Office Block, Hotel Equatorial Shanghai
No.65, Yan An Road (West), Shanghai, 200040, China
中国上海市延安西路65号上海国际贵都大饭店办公楼405单元
Phone: +86-21-62489820
Fax: +86-21-62489821